JOURNAL OF GUIDANCE, CONTROL, AND DYNAMICS
Vol. 24, No. 4, July–August 2001

Fixed-Range Optimal Trajectories of Supersonic Aircraft by First-Order Expansions

Robert Windhorst* and Mark Ardema†
Santa Clara University, Santa Clara, California 95053
and
David Kinney‡
NASA Ames Research Center, Moffett Field, California 94035

A near-optimal guidance law that generates minimum-fuel, minimum-time, or direct operating cost fixed-range trajectories for supersonic transport aircraft is developed. The approach uses singular perturbation techniques to timescale decouple the equations of motion into three sets of dynamics, two of which are studied here: weight/range and energy. The two-point boundary-value problems obtained by application of the maximum principle to the dynamic systems are solved using the method of matched asymptotic expansions. Both the weight/range and the energy dynamic solutions are carried out to first order. The two solutions are combined using the matching principle to form a uniformly valid approximation of the full fixed-range trajectory. Results show that the minimum-fuel trajectory has three segments: a minimum-fuel energy climb, a cruise climb, and a minimum-drag glide. The minimum-time trajectory also has three segments: a maximum dynamic pressure climb, a constant altitude cruise, and a maximum dynamic pressure descent. The minimum direct operating cost trajectory is an optimal combination of the preceding two trajectories. It is shown that for representative costs of fuel and flight time, the minimum direct operating cost trajectory is very similar to the minimum-fuel trajectory.

Nomenclature

D = drag
E = mechanical energy height
F = normalized tangential force
f = new state variable
g = gravity constant
H = Hamiltonian
h = altitude
J = cost functional
K_1 = cost of time
K_2 = cost of fuel
L = lift
M = Mach number
m = mass
N = normal load factor
q = dynamic pressure
R = final range
T = thrust
t = time
u = controls
v = velocity
w = weight
x = distance
α = angle of attack
β = fuel flow rate
γ = flight-path angle
ε = small parameter
η = dummy integration variable
λ_x = x adjoint variable
π = throttle
ρ = air density
τ = stretched time
ϕ = augmented cost integrand
ϕ_0 = cost integrand
$()_x$ = partial derivative with respect to x

Subscripts

0 = zero-order term
1 = first-order term

Superscripts

i = inner solution
o = outer solution
0 = ascent trajectory segment
1 = descent trajectory segment

Received 10 December 1999; revision received 23 October 2000; accepted for publication 25 October 2000.

*Research Assistant, Mechanical Engineering Department. Member AIAA.
†Professor of Mechanical Engineering, Mechanical Engineering Department. AIAA Fellow.
‡Aerospace Engineer, Systems Analysis Branch. Senior Member AIAA.

Introduction

THE high-speed civil transport (HSCT) has long been viewed as the ideal aircraft for long-distance routes, and, although this promising concept has been extensively researched in the past, it still has yet to see fruition in the airline market. One of the primary reasons for this is poor cost efficiency. With current technology, an HSCT design that is cost efficient enough to compete with subsonic transports while still meeting noise requirements may not be obtainable.[1–3] As technology advances, the search continues for a HSCT design with the fuel efficiency and payload capacity to make it viable in today's highly competitive airline market.

A key aspect of the fuel efficiency and payload capacity of an aircraft is its trajectory. There are many trajectories that will basically satisfy a given mission, but what is desired is an optimal trajectory that satisfies the mission constraints while, for example, consuming the least amount of fuel or requiring the least amount of time. A trajectory consuming the optimum combination of fuel and time produces the least direct operating cost to the airline for a given mission. This paper focuses on the problem of generating minimum-fuel, minimum-time, and minimum direct operating cost fixed-range trajectories for an HSCT. The goal is to develop a guidance algorithm for generating optimal trajectories that can be used within a design synthesis code.

To avoid the cost of building every proposed aircraft design, design synthesis computer codes have been developed to evaluate new designs in an efficient and inexpensive manner. For example, the NASA Ames Research Center ACSYNT[4] code combines

aerodynamic, propulsion, structure, weight, and mission aspects of aircraft design into a single optimization code. It computes converged and optimized vehicles, that is, vehicles whose weight has converged to the exact amount required for a specific mission and whose parameters are iteratively optimized to minimize a performance criterion. Included within ACSYNT is a subroutine that first generates a trajectory for each mission segment and then simulates the vehicle flying these segments by integrating the vehicle's equations of motion. This trajectory routine may be called many times while computing a converged and optimized vehicle. Because of these iterations, the trajectory routine must be fast, efficient, and robust. In the past, ACSYNT has used simple, nonoptimal flight paths in its trajectory routine. The guidance algorithm developed here is to be inserted into the trajectory routine for the purpose of generating not just any trajectory, but optimal trajectories that satisfy mission requirements and constraints.

Optimal trajectories may be obtained by direct or indirect methods. In the indirect method, the maximum principle is applied to a given dynamic model and associated cost function, and a two-point boundary-value problem (2PBVP) is obtained. Typically, as is true for our case, the 2PBVP is nonlinear (without an analytical solution), of twice the order of the original dynamic model, and unstable, making this a very difficult problem to solve. Numerical solution of the 2PBVP requires a large amount of iteration and designer insight for tuning numerical parameters to prevent the solution from diverging. The constrictive requirements of the design synthesis code preclude the use of an iterative numerical solution; therefore, we use a different technique to solve the 2PBVP in the guidance algorithm.

Singular perturbation techniques for solving nonlinear dynamic systems have been in use since before the advent of computers and numerical algorithms. These techniques break up the coupled full system of equations into a series of smaller and simpler systems. Each smaller system is solved separately, and the separate solutions are added back together to form a composite approximation of the solution of the full system. Notable successes of perturbation techniques have been in fluids, vibrations, celestial mechanics, and power systems.

The structure of a fixed-range transport aircraft trajectory is extremely well suited for analysis by singular perturbation methods. The trajectory naturally consists of three different segments: ascent, cruise, and descent. For supersonic aircraft, there may be an additional segment, a rapid transition in the ascent due to the transonic drag rise near $M = 1$. This altitude jump segment was analyzed in Ref. 5 and will not be considered here. The cruise segment of the trajectory is named the outer problem and is modeled as weight/range dynamics. It is assumed to evolve on a separate time scale from the ascent and descent segments. The cruise time scale is the natural time. On the other hand, the ascent and descent segments of the trajectory evolve on a stretched timescale and are appropriately called the boundary-layer or inner problems, which are modeled as energy dynamics. The guidance algorithm capitalizes on this timescale separation of the fixed range trajectory into separate segments using different independent variables for time.

Bryson et al.,[6] Kelly and Edelbaum,[7] and Kelly[8] noticed that the velocity and altitude state variables of a particular dynamic model of an aircraft were not timescale separable. They proposed a change of state variables such that the new states were timescale separable, and they substituted the velocity state with a new state known as specific energy or energy height. Furthermore, Kelly et al.[9] introduced a new state variable f to replace the altitude state, and Ardema and Rajan[10] derived examples of f along different segments of the energy climb path.

In Refs. 11 and 12, Ardema developed an approach for using singular perturbations and matched asymptotic expansions to timescale separate dynamic systems and approximated their optimal trajectories. Moreover, these references contain the details of the approach used in this paper. Ardema et al.,[5] Ardema,[13] and Calise[14–16] used this approach to solve aircraft flight performance problems. In some cases the approach allowed elimination of the 2PBVP arising from application of the maximum principle and derivation of the control as a function of state (state feedback control). References 13 and 16 illustrate one procedure for matching and combining the outer and inner solutions. A matched and combined outer and inner solution is formed twice: once for the initial boundary and once for final boundary. Then these two solutions are patched together using a condition at the intersection point. However, in Ref. 12 the initial boundary, outer solution, and final boundary are all combined at once using a single additive composite approximation. This composite approximation is what is used in this paper.

Erzberger and Lee[17] and Erzberger[18,19] developed an algorithm that generates optimum fixed-range trajectories for subsonic aircraft. The algorithm uses zero-order terms only and assumes constant weight. It is part of the avionics software used onboard subsonic transports today. Erzberger and Lee also introduced the minimum direct operating cost case by choosing a linear combination of time and fuel rate as the cost integrand. Time rate was multiplied by a constant representing the cost of time, and fuel rate was multiplied by a constant representing the cost of fuel.

Aggarwal et al.[20] solved the fixed-range optimal trajectory problem to first order in the inner problem and zero order in the outer problem. They solved the minimum-fuel case only. The dynamic model had weight and range on the same timescale. Results for a C-141 aircraft for both short- and long-range trajectories were given. It was shown that the first-order inner problem terms correct for distance and fuel consumed during ascent and descent.

In Ref. 5, the fixed-range optimal trajectory problem was solved to zero order in the outer and inner problems using a simplified dynamic model. In this dynamic model the weight of the aircraft was constant. In addition, the dynamic model was fully timescale separated; that is, each of the state variables of interest had its own timescale. The full timescale separation of the problem leads to elimination of the 2PBVP and control in state feedback form.

In the present paper, we adopt the singularly perturbed model of Ref. 20. This model is not fully timescale separable, and the 2PBVP can not be completely avoided. The fixed-range optimal trajectory problem is solved to first order in the outer and inner problems, and the outer and inner solutions are combined into an additive composite approximation of the optimal trajectory. The guidance algorithm calculates the control as a function of state and one unknown boundary condition. This is the first time this dynamic model has been completely solved to first order for fixed-range problems, and it is the first time the single additive composite approximation of Ref. 12 has been used in solving the fixed-range problem. Also, this is the first application of this method to supersonic aircraft trajectories.

Problem Statement

The singularly perturbed dynamic model comprises five state variables: w, x, E, h, and γ. It models the vertical plane dynamics only and assumes a flat, nonrotating Earth. Also, $\cos\gamma$ and $\sin\gamma$ terms are eliminated using the small-angle approximation. The throttle setting π is assumed to be a bounded control, and N is assumed to be an unbounded control. The fixed-range optimal trajectory problem is set up as a singularly perturbed dynamic model,

$$\dot{w} = -\beta, \qquad \dot{x} = v, \qquad \varepsilon\dot{E} = vF$$
$$\varepsilon^2\dot{h} = v\gamma, \qquad \varepsilon^2\dot{\gamma} = (g/v)(N-1) \tag{1}$$

where

$$v = \sqrt{2g(E-h)}, \qquad F = (T\cos\alpha - D)/w$$
$$N = (T\sin\alpha + L)/w$$

The associated cost functional is

$$J = \int_0^{t_f} (K_1 + K_2\beta)\,\mathrm{d}t \tag{2}$$

Different powers of ε in Eqs. (1) denote different timescales. Clearly, w and x remain on the same timescale as do h and γ. The weight/range and energy timescales will be solved to first order. The altitude/flight-path angle timescale will not be considered in this paper. In Eq. (2) we follow Erzberger and Lee[17] and denote K_1 as the cost of time and K_2 as the cost of fuel.

The fixed-range trajectory problem is bounded by several state and control constraints. The M upper limit is 2.4, and the q upper limit is 1000 lb/ft^2. The h lower limit is 1500 ft, and the h upper

limit is 60,000 ft. Also, π is bounded by maximum thrust, $\pi = 1$, and idle. Idle is the minimum allowable power level the pilot can set the engine to while in the air. If the power level is set lower than idle, then there exists a risk that the engine flame could be extinguished. Here β is a non-linear function of π, h, and M. Finally, the standard 250-kn maximum speed under 10,000 ft imposed by air traffic control is ignored.

The Hamiltonian is formed as

$$H = -K_1 - \bar{\lambda}\beta + \lambda_x v + \lambda_E v F + \lambda_h v\gamma + \lambda_\gamma (g/v)(N-1) \tag{3}$$

where

$$\bar{\lambda} = K_2 + \lambda_w \tag{4}$$

Using Eq. (3), we form the adjoint differential equations

$$\dot{\lambda}_w = -\lambda_E v F_w, \qquad \dot{\lambda}_x = 0$$

$$\varepsilon\dot{\lambda}_E = \bar{\lambda}\beta_E - \lambda_x v_E - \lambda_E(v_E F + v F_E) - \lambda_h v_E \gamma + \lambda_\gamma (g/v^2)(N-1)v_E$$

$$\varepsilon^2\dot{\lambda}_h = \bar{\lambda}\beta_h - \lambda_x v_h - \lambda_E(v_h F + v F_h) - \lambda_h v_h \gamma + \lambda_\gamma (g/v^2)(N-1)v_h$$

$$\varepsilon^2\dot{\lambda}_\gamma = -\lambda_h v \tag{5}$$

where F_w, for example, is the partial derivative of F with resect to w. Each adjoint equation is multiplied by the same power of ε as its corresponding state equation in Eqs. (1) (Ref. 5). The state boundary conditions are

$$w(0) = w_0, \qquad x(0) = 0, \qquad E(0) = E_0, \qquad h(0) = h_0$$

$$\gamma(0) = \gamma_0, \qquad w(t_f) = \text{free}, \qquad x(t_f) = R$$

$$E(t_f) = E_f, \qquad h(t_f) = h_f, \qquad \gamma(t_f) = \gamma_f \tag{6}$$

where t_f is free. The transversality conditions provide the adjoint boundary conditions,

$$\bar{\lambda}(0) = \lambda_x(0) = \lambda_E(0) = \lambda_h(0) = \lambda_\gamma(0) = \text{free}$$

$$\bar{\lambda}(t_f) = K_2, \qquad \lambda_x(t_f) = \lambda_E(t_f) = \lambda_h(t_f) = \lambda_\gamma(t_f) = \text{free} \tag{7}$$

The maximum principle provides two necessary conditions for optimal control:

$$H = 0, \qquad u = \arg\max_{u \in \cup}[H] \tag{8}$$

where U is the set of all admissible controls. The second of Eqs. (8) is used to find the controls and is valid for bounded or unbounded controls.

Eqs. (1) and (5–8) make up a nonlinear 2PBVP of order 10. There are 12 variables: 5 states, 5 adjoints, and 2 controls. For each state and adjoint variable there is a first-order differential equation [Eqs. (1) and (5)], with associated boundary conditions [Eqs. (6) and (7)]. Note that exactly half of the boundary conditions are initial and half are final.

The following procedure reduces the 2PBVP by an order of one and replaces one of the adjoint differential equations in Eqs. (5) by the first of Eqs. (8). First choose the adjoint to be replaced, for example, λ_j. Then group the Hamiltonian into the form

$$H = -\phi + \lambda_j f_j$$

where

$$\phi = \phi_0 - \sum_{\substack{i=1 \\ i \neq j}}^{n} \lambda_i f_i$$

and where f_i is the state equation corresponding to λ_i and ϕ_0 is the integrand of J. Now the conditions in Eqs. (8) may be stated differently, but equivalently, as follows[21]:

$$\lambda_j = \phi/f_j, \qquad u = \arg\min_{u \in \cup}[\phi/|f_j|] \tag{9}$$

Timescale separation of Eqs. (1) and (5) creates three reduced-order systems, only the first two of which are of interest here. The outer problem or weight/range dynamics evolves in regular time t, and the inner problem or energy dynamics evolves in stretched time, $\tau = t/\varepsilon$. Once timescale separated, each system is expanded in powers of ε, retaining only zero- and first-order terms. Finally, coefficients of like powers in ε are grouped together, forming four sets of equations: zero-order weight/range dynamics, first-order weight/range dynamics, zero-order energy dynamics, and first-order energy dynamics. The process of timescale decoupling and expansion of the equations is explained in detail in Ref. 11, but here we simply state the resulting equations in Appendices A–E. The superscript o denotes that the variable is associated with the outer problem, weight/range dynamics, and the superscript i denotes that the variable is associated with the inner problem, energy dynamics. The subscripts denote whether the variable is zero order or first order. The equations in Appendices A–E are used to produce the major results that will make up the algorithm.

Zero-Order Weight/Range Dynamics

Equations (A1) and (A2) (see Appendix A) contain six functions,

$$F_0^o = 0, \qquad \gamma_0^o = 0, \qquad N_0^o = 1, \qquad \lambda_{h0}^o = 0$$

$$\bar{\lambda}_0^o \beta_{E0}^o = \lambda_{x0}^o v_{E0}^o + \lambda_{E0}^o v_0^o F_{E0}^o, \qquad \bar{\lambda}_0^o \beta_{h0}^o = \lambda_{x0}^o v_{h0}^o + \lambda_{E0}^o v_0^o F_{h0}^o \tag{10}$$

The first 4 of Eqs. (10) can be used to calculate 4 of the 12 variables. In addition to the six functions, Eqs. (A1) and (A2) contain four first-order differential equations with boundary conditions: two state equations,

$$\frac{\mathrm{d}w_0^o}{\mathrm{d}t} = -\beta_0^o, \qquad w_0^o(0) = C_0^w = w_0, \qquad w_0^o(0) = \text{free}$$

$$\frac{\mathrm{d}x_0^o}{\mathrm{d}t} = v_0^o, \qquad x_0^o(0) = C_0^x = x_0, \qquad x_0^o(t_f) = R \tag{11}$$

and two adjoint equations,

$$\frac{\mathrm{d}\bar{\lambda}_0^o}{\mathrm{d}t} = -\lambda_{E0}^o v_0^o F_{w0}^o, \qquad \bar{\lambda}_0^o(0) = \text{free}, \qquad \bar{\lambda}_0^o(t_f) = C_0^{\bar{\lambda}} = K_2$$

$$\frac{\mathrm{d}\lambda_{x0}^o}{\mathrm{d}t} = 0, \qquad \lambda_{x0}^o(0) = \lambda_{x0}^o(t_f) = C_0^{\lambda_x} = \text{free} \tag{12}$$

The C are free constants of integration used to match the weight/range solution to the energy solutions. The section on matching shows how the C relate to the state boundary conditions.

The third of Eqs. (10) and first of Eqs. (11) constitute two relations for calculating N and w. Because $F = f(w, E, h, N, \pi)$, two of the three variables E, h, and π must be given to calculate the third. We choose to use the necessary conditions of Eqs. (9) to generate E and h. Consequently, π is found using $F = 0$, from Eqs. (10).

Substituting the first three of Eqs. (10) into Eq. (3) results in the zero-order weight/range Hamiltonian equation,

$$H_0^o = -K_1 - \bar{\lambda}_0^o \beta_0^o + \lambda_{x0}^o v_0^o = 0$$

Note that in Eqs. (12), all of the boundary conditions except one are free unknown constants to be determined by the 2PBVP, and the known constant is given at t_f. Furthermore, λ_x is constant for all t. The preceding conditions plus the alternate form of the necessary conditions in Eqs. (9) suggest the following algorithm for calculating zero-order weight/range dynamic variables:

1) Guess the final weight of the aircraft w_f.

2) Choose λ_x as λ_j in Eqs. (9). Evaluate the control variables and λ_x at t_f using w_f from step 1, Eqs. (10), and the following:

$$\lambda_{x0}^o = \frac{\phi}{f} = \frac{K_1 + K_2\beta_0^o(t_f)}{v_0^o(t_f)}$$

$$\left.\begin{matrix} E_0^o \\ h_0^o \end{matrix}\right\} = \arg\min_{E,h \in \cup} \left[\frac{K_1 + K_2\beta_0^o}{|v_0^o|}\right]_{\substack{F_0^o = 0 \\ \gamma_0^o = 0 \\ N_0^o = 1}} \tag{13}$$

where $\bar{\lambda}_0^o(t_f) = K_2$ from Eqs. (12).

3) Choose $\bar{\lambda}$ as λ_j in Eqs. (9). Begin evaluation of the control variables and $\bar{\lambda}$ beginning at t_0 and moving on to subsequent t using Eqs. (10) and the following:

$$\bar{\lambda}_0^o = \frac{\phi}{f} = \frac{K_1 - \lambda_{x0}^o v_0^o}{-\beta_0^o}$$

$$\left.\begin{matrix} E_0^o \\ h_0^o \end{matrix}\right\} = \arg \min_{E,h \in \cup} \left[\frac{K_1 - \lambda_{x0}^o v_0^o}{\left|\beta_0^o\right|} \right]_{\substack{F_0^o = 0 \\ \gamma_0^o = 0 \\ N_0^o = 1}} \tag{14}$$

where λ_x is given by Eqs. (13). Once the control variables are calculated at a given t, integrate Eqs. (11) to find the states at the next t.

4) When w_f from step 1 is reached, stop. Proceed by calculating the first-order weight/range, zero-order energy, and first-order energy solutions. Match the inner and outer solutions, and form the additive composite approximation. Check to see if the composite approximation range matches the desired range; if not, determine a new w_f by a suitable one-dimensional search procedure, and repeat the process until convergence is obtained.

The preceding procedure does not eliminate the 2PBVP, but it does result in a relatively simple one. The procedure simplifies the problem in that only one unknown boundary condition, w_f, must be guessed instead of two, λ_x and $\bar{\lambda}$. In practice, the iteration could be avoided by making a graph or table of precomputed w_f vs R for a given aircraft. The desired w_f could then be found from the table or graph.

It can be shown that Eqs. (14) give the same controls as do the fourth and fifth of Eqs. (10), and that Eqs. (13) are the same as the fourth and fifth of Eqs. (10) evaluated at t_f (Ref. 21).

The zero-order weight/range dynamics have two special cases: minimum time and minimum fuel; these will be discussed now.

Minimum Time, $K_1 = 1$ and $K_2 = 0$

Substituting the preceding values of K_1 and K_2 and the adjoint into the optimization functions in Eqs. (13) and (14) produces the following simplified optimization functions:

$$\frac{1}{v_0^o(t_f)} \tag{15a}$$

from Eqs. (13), and

$$\frac{v_0^o(t_f) - v_0^o}{\beta_0^o v_0^o(t_f)} \tag{15b}$$

from Eqs. (14).

Recall that the optimization function in Eqs. (13) is minimized at t_f and that the optimization function in Eqs. (14) is minimized at all t. Therefore, Eqs. (13) produce controls maximizing v at t_f, and Eqs. (14) produce controls that drive the current v to the final optimum v at t_f and maximize β. This solution makes sense because to reach a destination in minimum time, one travels at maximum speed. Furthermore, it is desirable to burn off fuel quickly to minimize D.

Minimum Fuel, $K_1 = 0$ and $K_2 = 1$

Substitution of the preceding values of K_1 and K_2, and the adjoint into the optimization functions in Eqs. (13) and (14) produces the following simplified optimization functions:

$$\frac{\beta_0^o(t_f)}{v_0^o(t_f)} \tag{16a}$$

from Eqs. (13), and

$$-\frac{\beta_0^o(t_f)}{v_0^o(t_f)} \frac{v_0^o}{\beta_0^o} \tag{16b}$$

from Eqs. (14).

Again, recall that the optimization function in Eqs. (13) is minimized at t_f and that the optimization function in Eqs. (14) is minimized at all t. Minimizing the ratio β/v is equivalent to maximizing the Breguet factor (see Ref. 5), provided β is a linear function of π (not assumed in this paper). Equations (13) produce controls that minimize β/v at t_f, and Eqs. (14) produce controls that minimize β/v and drive the current β/v to the optimum β/v at t_f. This solution makes sense because to reach a destination using a minimum amount of fuel one travels such that the fuel burned per distance gained, β/v, is minimized.

First-Order Weight/Range Dynamics

Substitution of Eqs. (10) into Eqs. (B1) (see Appendix B) produces the following three algebraic relations:

$$F_1^o = \frac{1}{v_0^o} \frac{\mathrm{d}E_0^o}{\mathrm{d}t}, \qquad \gamma_1^o = 0, \qquad N_1^o = 0 \tag{17}$$

Substitution of Eqs. (10) and (17) into Eqs. (B2) produces the following three algebraic relations:

$$\frac{\mathrm{d}\lambda_{E0}^o}{\mathrm{d}t} = \bar{\lambda}_1^o \beta_{E0}^o + \bar{\lambda}_0^o \beta_{E1}^o - \lambda_{x1}^o v_{E0}^o - \lambda_{x0}^o v_{E1}^o - \lambda_{E1}^o v_0^o F_{E0}^o - \lambda_{E0}^o \left(v_{E0}^o F_1^o + v_1^o F_{E0}^o + v_0^o F_{E1}^o \right)$$

$$0 = \bar{\lambda}_1^o \beta_{h0}^o + \bar{\lambda}_0^o \beta_{h1}^o - \lambda_{x1}^o v_{h0}^o - \lambda_{x0}^o v_{h1}^o - \lambda_{E1}^o v_0^o F_{h0}^o - \lambda_{E0}^o \left(v_{h0}^o F_1^o + v_1^o F_{h0}^o + v_0^o F_{h1}^o \right)$$

$$\lambda_{h1}^o v_0^o = 0 \tag{18}$$

Substitution of Eqs. (10) and (17) into Eqs. (E2) produces the following three relations from the first-order necessary conditions for optimal control (recall that N is unbounded),

$$\bar{\lambda}_1^o \beta_0^o + \bar{\lambda}_0^o \beta_1^o = \lambda_{x1}^o v_0^o + \lambda_{x0}^o v_1^o + \lambda_{E0}^o v_0^o F_1^o$$

$$\lambda_{E1}^o v_0^o F_{N0}^o + \lambda_{E0}^o \left(v_1^o F_{N0}^o + v_0^o F_{N1}^o \right) = \lambda_{\gamma 0}^o \left(g / v_0^{o^2} \right) v_1^o - \lambda_{\gamma 1}^o \left(g / v_0^o \right)$$

$$\bar{\lambda}_1^o \beta_{\pi 0}^o + \bar{\lambda}_0^o \beta_{\pi 1}^o = \lambda_{E1}^o v_0^o F_{\pi 0}^o + \lambda_{E0}^o \left(v_1^o F_{\pi 0}^o + v_0^o F_{\pi 1}^o \right) \tag{19}$$

Eight of nine relations in Eqs. (17–19) are used to calculate eight first-order variables. The remaining four come from the first-order differential equations in Eqs. (B1) and (B2): two state equations with solutions,

$$w_1^o = -\int_0^t \left(\beta_{E0}^o E_1^o + \beta_{h0}^o h_1^o + \beta_{\pi 0}^o \pi_1^o \right) \mathrm{d}\eta + C_1^w$$

$$x_1^o = \int_0^t \frac{g}{v_0^o} \left(E_1^o - h_1^o \right) \mathrm{d}\eta + C_1^x \tag{20}$$

and two adjoint equations with solutions,

$$\bar{\lambda}_1^o = -\int_0^t \left[\lambda_{E1}^o v_0^o F_{w0}^o + \lambda_{E0}^o \left(v_1^o F_{w0}^o + v_0^o F_{w1}^o \right) \right] \mathrm{d}\eta + C_1^{\bar{\lambda}}$$

$$\lambda_{x1}^o = \text{const} = C_1^{\lambda_x} \tag{21}$$

where the constants C will be determined later by the matching condition. In principle there are 12 equations and 12 variables, and, thus, the problem can be solved. Unfortunately, Eqs. (17–19) contain terms having second-order partial derivatives, for example,

$$F_{E1}^o = F_{Ew0}^o w_1^o + F_{EE0}^o E_1^o + F_{Eh0}^o h_1^o + F_{EN0}^o N_1^o + F_{E\pi 0}^o \pi_1^o$$

In ACSYNT, the aerodynamic variables are calculated by different methods depending on which zone in the flight envelope the airplane is located in. Using these different methods causes small discontinuities in the aerodynamic variables at the zone boundaries, making the calculation of second-order partial derivatives difficult and, in general, unreliable.

To make the solutions of Eqs. (17–19) tractable, two assumptions are now made. First, it is assumed that optimal cruise flight is at full throttle and, thus, $\pi_0^o = 1$ and $\pi_1^o = 0$. Second, it is assumed that the cruise speed is always on the upper M boundary of the flight envelope. Both of these assumptions must be checked for validity in any numerical solution.

According to the standard atmospheric model, the speed of sound is constant for the span of altitudes encompassing the M bound.

Therefore, we can replace the M bound by a velocity bound, and we add the following state constraint to the problem:

$$\sqrt{2g(E^o - h^o)} - v_{\max} \leq 0 \tag{22}$$

Equation (22) is adjoined to the Hamiltonian by a multiplier μ, with the property

$$v < v_{\max} \Rightarrow \mu = 0, \qquad v = v_{\max} \Rightarrow \mu \neq 0 \tag{23}$$

Expanding Eq. (22) in powers of ε produces

$$E_0^o + \varepsilon E_1^o = \left(v_{\max}^2 \big/ 2g\right) + h_0^o + \varepsilon h_1^o \tag{24}$$

Equating terms in Eq. (24) with like powers of ε yields

$$E_1^o = h_1^o \tag{25}$$

Now expand F, substitute in Eq. (25), and use the third of Eqs. (17) to get

$$F_1^o = F_{w0}^o w_1^o + E_1^o\left(F_{E0}^o + F_{h0}^o\right) \tag{26}$$

Substituting Eq. (26) into the first of Eqs. (17) and solving for E give

$$E_1^o = \frac{1}{\left(F_{E0}^o + F_{h0}^o\right)}\left[\frac{1}{v_0^o}\frac{\mathrm{d}E_0^o}{\mathrm{d}t} - F_{w0}^o w_1^o\right] \tag{27}$$

Finally, substitution of Eqs. (25) and (27) into Eqs. (20) produces

$$w_1^o = -\int_0^t \frac{\left(\beta_{E0}^o + \beta_{h0}^o\right)}{\left(F_{E0}^o + F_{h0}^o\right)}\left[\frac{1}{v_0^o}\frac{\mathrm{d}E_0^o}{\mathrm{d}t} - F_{w0}^o w_1^o\right]\mathrm{d}\eta + C_1^w$$

$$x_1^o = C_1^x \tag{28}$$

A possible interpretation of w_1^o is that it is a correction to the vehicle weight accounting for extra fuel burned while the vehicle slowly gains energy and altitude during the cruise trajectory segment. Recall that although $F = 0$ in the zero-order solution, E can change because it is used as a control. Here w_0^o accounts only for fuel burned in steady-state flight at each altitude point during the cruise segment; it does not take into account extra fuel required in transient flight to the next altitude point.

Zero-Order Energy Dynamics

Equations (C1) and (C2) contain the following constant variables:

$$w_0^i = \begin{cases} w_0, \text{ ascent} \\ w_f, \text{ descent} \end{cases} \qquad x_0^i = \begin{cases} 0, \text{ ascent} \\ R, \text{ descent} \end{cases}$$

$$\bar{\lambda}_0^i = \begin{cases} \dfrac{K_1 - \lambda_{x0}^o v_0^o(0)}{-\beta_0^o(0)}, & \text{ascent} \\ K_2, & \text{descent} \end{cases}$$

$$\lambda_{x0}^i = \frac{K_1 + K_2\beta_0^o(t_f)}{v_0^o(t_f)}, \text{ ascent and descent} \tag{29}$$

and provide the following four additional relations:

$$\gamma_0^i = 0, \qquad N_0^i = 1, \qquad \lambda_{h0}^i = 0$$

$$\bar{\lambda}_0^i \beta_{h0}^i = \lambda_{x0}^i v_{h0}^i + \lambda_{E0}^i\left(v_{h0}^i F_0^i + v_0^i F_{h0}^i\right) \tag{30}$$

Furthermore, there are two differential equations

$$\frac{\mathrm{d}E_0^i}{\mathrm{d}\tau} = v_0^i F_0^i, \qquad \frac{\mathrm{d}\lambda_{E0}^i}{\mathrm{d}\tau} = \bar{\lambda}_0^i \beta_{E0}^i - \lambda_{x0}^i v_{E0}^i - \lambda_{E0}^i\left(v_{E0}^i F_0^i + v_0^i F_{E0}^i\right) \tag{31}$$

with boundary conditions depending on whether the trajectory segment is ascent

$$E_0^i(\tau^1 = 0) = E_0, \qquad E_0^i(\tau^1 \to \infty) = E_0^o(0)$$

$$\lambda_{E0}^i(\tau^1 = 0) = \text{free}, \qquad \lambda_{E0}^i(\tau^1 \to \infty) = \lambda_{E0}^o(0) \tag{32}$$

or descent

$$E_0^i(\tau^2 \to \infty) = E_0^o(t_f), \qquad E_0^i(\tau^2 = 0) = E_f$$

$$\lambda_{E0}^i(\tau^2 \to \infty) = \lambda_{E0}^o(t_f), \qquad \lambda_{E0}^i(\tau^2 = 0) = \text{free} \tag{33}$$

where $\tau^1 = t/\varepsilon$ and $\tau^2 = (t_f - t)/\varepsilon$. Compliance with the boundary conditions in Eqs. (32) and (33) requires that vF must satisfy the following inequality constraint[21]:

$$vF \begin{cases} > 0, & \text{ascent} \\ < 0, & \text{descent} \end{cases}$$

Substituting the first two of Eqs. (30) into Eq. (3) results in the zero-order energy Hamiltonian equation,

$$H_0^i = -K_1 - \bar{\lambda}_0^i \beta_0^i + \lambda_{x0}^i v_0^i + \lambda_{E0}^i v_0^i F_0^i = 0$$

For the energy dynamics, we calculate π and h using the necessary conditions from Eqs. (9). Choosing λ_E as λ_j yields

$$\lambda_{E0}^i = \frac{\phi}{f} = \frac{K_1 + \bar{\lambda}_0^i \beta_0^i - \lambda_{x0}^i v_0^i}{v_0^i F_0^i}$$

$$\left.\begin{matrix} h_0^i \\ \pi_0^i \end{matrix}\right\} = \arg\min_{h,\pi \in \cup}\left[\frac{K_1 + \bar{\lambda}_0^i \beta_0^i - \lambda_{x0}^i v_0^i}{\left|v_0^i F_0^i\right|}\right]_{\substack{\gamma_0^i = 0 \\ N_0^i = 1}} \tag{34}$$

where $\gamma = 0$ and $N = 1$ come from Eqs. (30). The equivalence of Eqs. (34) to the last of Eqs. (30) and the first of Eqs. (E1) is shown in Ref. 21.

The zero-order energy dynamics solution has four special cases of interest: minimum-time ascent, minimum-fuel ascent, minimum-time descent, and minimum-fuel descent. After substituting in the values of the constants and adjoints, the simplified optimization functions can be separated into two parts. One part drives the states and controls of the inner problem toward the state and control boundaries of the outer problem, and the other part optimizes the cost.

Minimum Time, $K_1 = 1$ and $K_2 = 0$

Substituting K_1 and K_2 and adjoints from Eqs. (29) into Eqs. (34) produces the following simplified optimization functions:

For ascent, $vF > 0$

$$\frac{\beta_0^o(0)\left[v_0^o(t_f) - v_0^i\right] - \beta_0^i\left[v_0^o(t_f) - v_0^o(0)\right]}{\beta_0^o(0) v_0^o(t_f)} * \frac{1}{\left|v_0^i F_0^i\right|} \tag{35}$$

For descent, $vF < 0$

$$\frac{v_0^o(t_f) - v_0^i}{v_0^o(t_f)} * \frac{1}{\left|v_0^i F_0^i\right|} \tag{36}$$

Recall that Eqs. (34) stipulate controls minimizing Eqs. (35) and (36). The term on the left in Eq. (35) drives the ascent states and controls to those at the beginning of cruise. Likewise, the term on the left in Eq. (36) drives the descent states and controls to those at the end of cruise. Furthermore, the term on the right in both equations produces controls that maximize the absolute value of the specific excess power of the vehicle. The actual controls chosen depend on the product of the left and right terms. Typically, the right term dominates the choice of controls unless cruise is close by. When cruise is near, then the left term dominates.

The restrictions on vF, in effect, impose two different constraints on π for ascent and descent. For example, during ascent, the only allowable throttles are those that produce T greater then D. The opposite is true for descent. Because the rightmost term maximizes the absolute value of the specific excess power of the vehicle, π is at or near maximum during ascent and at or near idle during descent. The very low π during descent causes F to behave like D [see Eqs. (1)]. Thus, vD is approximately maximized during descent.

The terms on the left in Eqs. (35) and (36) are always positive. During ascent, the optimization function equals a positive value that

decreases until it reaches zero at the beginning of cruise. Conversely, during descent, the optimization function begins equal to zero, end of cruise, and increases from there.

Minimum Fuel, $K_1 = 0$ and $K_2 = 1$

Substituting K_1 and K_2 and adjoints from Eqs. (29) into Eqs. (34) produces the following simplified optimization functions:

For ascent, $vF > 0$

$$\frac{\beta_0^o(t_f)}{v_0^o(t_f)}\left(\frac{v_0^o(0)}{\beta_0^o(0)} - \frac{v_0^i}{\beta_0^i}\right) * \frac{\beta_0^i}{\left|v_0^i F_0^i\right|} \tag{37}$$

For descent, $vF < 0$

$$\frac{\beta_0^o(t_f)}{v_0^o(t_f)}\left(\frac{v_0^o(t_f)}{\beta_0^o(t_f)} - \frac{v_0^i}{\beta_0^i}\right) * \frac{\beta_0^i}{\left|v_0^i F_0^i\right|} \tag{38}$$

Again, Eqs. (34) stipulate controls minimizing Eqs. (37) and (38). Similar to the minimum-time case, the terms on the left drive the states and controls of the energy dynamics solution toward the states and controls at the boundaries of the weight/range dynamics solution. Furthermore, the term on the right produces controls that minimize the ratio of fuel burned to energy gained. It is equivalent to the optimization function that produces the minimum-fuel energy-climb path.

During ascent, the term on the left produces controls that drive the ascent v/β ratio to v/β at the beginning of cruise. Because of the constraint on π that was discussed in the preceding minimum-time case, the ascent v/β approaches the cruise v/β from below, forcing the optimization function to always be positive. The descent case is different. Now the constraint on π allows very small β, that is, idle. At idle, β is small enough to drive the descent v/β larger than v/β at the end of cruise, where idle was not allowable due to $F = 0$. These descent and cruise v/β ratios make the term on the left of Eq. (38) negative. The negative sign changes the optimization process from a minimization to a maximization. Moreover, at idle π, the term on the right behaves like $1/vD$ because T is almost zero and β is small, making w almost constant. Therefore, maximizing the term on the right is equivalent to minimizing vD. Minimizing vD is the opposite result from what was derived for the minimum-time descent case, that is, maximizing vD.

First-Order Energy Dynamics

Equations (D1) and (D2) contain three functions,

$$\gamma_1^i = \frac{1}{v_0^i}\frac{\mathrm{d}h_0^i}{\mathrm{d}\tau}, \qquad N_1^i = \frac{v_0^i}{g}\frac{\mathrm{d}\gamma_0^o}{\mathrm{d}\tau}, \qquad \lambda_{h1}^i = -\frac{1}{v_0^i}\frac{\mathrm{d}\lambda_{\gamma 0}^i}{\mathrm{d}\tau} \tag{39}$$

and six differential equations whose solutions may be expressed in integral form as

$$w_1^i = -\int_0^\tau \beta_0^i \,\mathrm{d}\eta, \qquad x_1^i = \int_0^\tau v_0^i \,\mathrm{d}\eta$$

$$E_1^i = \int_0^\tau \left(v_1^i F_0^i + v_0^i F_1^i\right)\mathrm{d}\eta, \qquad \bar{\lambda}_1^i = -\int_0^\tau \lambda_{E0}^i v_0^i F_{w0}^i \,\mathrm{d}\eta$$

$$\lambda_{x1}^i = 0, \qquad \lambda_{E1}^i = \int_0^\tau \left(\bar{\lambda}_1^i \beta_{E0}^i + \cdots\right)\mathrm{d}\eta \tag{40}$$

Equations (39) and (40) provide 9 equations for solving for 9 of the 12 state, adjoint, and control variables. The other three variables can be calculated using the h adjoint equation in Eqs. (D2) and two of the three first-order necessary conditions in Eqs. (E2). Again, some of these equations contain terms having second-order partial derivatives. Fortunately, the two equations of interest in Eqs. (40), namely, the w and x equations, are easily solvable without the others. Notice that the only terms in these two integrals are of zero order and, thus, are known from the zero-order solutions. In fact, the first-order w and x terms can be interpreted as the obvious corrections to the zero-order solutions, which assumed a constant mass and range during the ascent and descent.

Matching and Composite Solution

Once the four systems of equations are solved, each solution must be combined such that their composite approximates the solution to the full system. A key aspect in this regard is that the inner solution must asymptotically approach the outer solution boundary as τ approaches infinity. This is accomplished by the matching principle. The matching principle is fully described in Refs. 11 and 12. Additionally, the matching principle gives a procedure for determining the unknown constants of integration, C. It may be stated mathematically as

$$\lim_{\substack{\varepsilon\to 0\\ t\to 0\\ \tau\to\infty}} \{y^o(\varepsilon, t) - y^i(\varepsilon, \tau)\} = 0 \tag{41}$$

where y represents any state variable. Note that ε must approach zero faster than t for τ to approach infinity.

Because we have two inner solutions, one for ascent and one for descent, we must apply Eq. (41) to each state twice. Following the procedure in Refs. 11 and 12, we apply the rule to our states w and x:

Ascent for w is

$$\lim_{\substack{\varepsilon\to 0\\ t\to 0\\ \tau^1\to\infty}} \left\{\begin{array}{l} C_0^w + \varepsilon C_1^w - t\beta_0^o(0) + \cdots \\ -w_0^{i1}(0) - \varepsilon I_w^{1^*} + t\beta_0^{i1}(\tau^1 \to \infty) + \cdots \end{array}\right\} = 0 \tag{42a}$$

and descent for w is

$$\lim_{\substack{\varepsilon\to 0\\ tf-t\to 0\\ \tau^2\to\infty}} \left\{\begin{array}{l} w_0^o(t_f) + \varepsilon w_1^o(t_f) + (t_f - t)\beta_0^o(t_f) + \cdots \\ -w_o^{i2}(0) - \varepsilon w_1^{i2}(0) + \varepsilon I_w^{2^*} - (t_f - t)\beta_0^{i2}(\tau^2 \to \infty) + \cdots \end{array}\right\}$$

$$= 0 \tag{42b}$$

Ascent for x is

$$\lim_{\substack{\varepsilon\to 0\\ t\to 0\\ \tau^1\to\infty}} \left\{\begin{array}{l} C_0^x + \varepsilon C_1^x + t v_0^o(0) + \cdots \\ -x_0^{i1}(0) + \varepsilon I_x^{1^*} - t v_0^{i1}(\tau^1 \to \infty) + \cdots \end{array}\right\} = 0 \tag{43a}$$

and descent for x is

$$\lim_{\substack{\varepsilon\to 0\\ t_f - t\to 0\\ \tau^2\to\infty}} \left\{\begin{array}{l} x_0^o(t_f) + \varepsilon x_1^o(t_f) - (t_f - t)v_0^o(t_f) + \cdots \\ -x_0^{i2}(0) - \varepsilon x_1^{i2}(0) - \varepsilon I_x^{2^*} + (t_f - t)v_0^{i2}(\tau^2 \to \infty) + \cdots \end{array}\right\}$$

$$= 0 \tag{43b}$$

where the dots stand for the omitted higher-order terms in the series and

$$I_w^{1^*} = \int_0^{\tau^1\to\infty} \left[\beta_0^{i1}(\infty) - \beta_0^{i1}\right]\mathrm{d}\eta$$

$$I_x^{1^*} = \int_0^{\tau^1\to\infty} \left[v_0^{i1}(\infty) - v_0^{i1}\right]\mathrm{d}\eta$$

$$I_w^{2^*} = \int_0^{\tau^2\to\infty} \left[\beta_0^{i2}(\infty) - \beta_0^{i2}\right]\mathrm{d}\eta$$

$$I_x^{2^*} = \int_0^{\tau^2\to\infty} \left[v_0^{i2}(\infty) - v_0^{i2}\right]\mathrm{d}\eta \tag{44}$$

Equating terms of like powers in εt yields

$$C_0^w = w_0^{i1}(0) = w_0, \qquad C_1^w = I_w^{1^*}, \qquad -\beta_0^o(0) = -\beta_0^{i1}(\tau^1 \to \infty)$$

$$w_0^o(t_f) = w_0^{i2}(0) = \text{ free}, \qquad w_1^o(t_f) = w_1^{i2}(0) - I_w^{2^*}$$

$$\beta_0^o(t_f) = (\tau^2 \to \infty)\beta_0^{i2}$$

$$C_0^x = x_0^{i1}(0) = x_0, \qquad C_1^x = -I_x^{1^*}, \qquad v_0^o(0) = v_0^{i1}(\tau^1 \to \infty)$$

$$x_0^o(t_f) = x_0^{i2}(0) = R, \qquad x_1^o(t_f) = x_1^{i2}(0) + I_x^{2*}$$

$$-v_0^o(t_f) = -v_0^{i2}(\tau^2 \to \infty)$$

where the boundary conditions satisfy Eqs. (6) and (29). Although not shown here, the adjoints are matched similarly.

Now we are ready to form the additive composite approximation[12]:

$$y^a(\varepsilon, t) = y^o(\varepsilon, t) + y^{i1}(\varepsilon, \tau^1) + y^{i2}(\varepsilon, \tau^2) - CP^1(\varepsilon, t) - CP^2(\varepsilon, t) \tag{45}$$

where the CP are terms common to both solutions and cancel out in Eqs. (42) and (43). After setting $\varepsilon = 1$, the additive composite approximation is formed. Substituting the weight/range and energy solutions into Eq. (45) and simplifying yield

$$w^a = w_0 - \int_0^t \left[\beta_0^o - \beta_0^o(0) - \beta_0^o(t_f)\right] \mathrm{d}\eta - \int_0^t \beta_0^{i1}\, \mathrm{d}\eta - \int_0^t \beta_0^{i2}\, \mathrm{d}\eta$$

$$x^a = x_0 + \int_0^t \left[v_0^o - v_0^o(0) - v_0^o(t_f)\right] \mathrm{d}\eta + \int_0^t v_0^{i1}\, \mathrm{d}\eta + \int_0^t v_0^{i2}\, \mathrm{d}\eta \tag{46}$$

$x^a(t_f)$ is equal to $x_0^o(t_f) - I_x^{1^*} - I_x^{2^*}$. Thus, in step 4 of the zero-order weight/range algorithm, we iterate until $x^a(t_f) = R^*$, where the asterisk denotes that this range is different from the R used to satisfy the final boundary condition. Similarly, additive compositions for E and h, if desired, are formed as

$$E^a = E_0^o + E_0^{i1} + E_0^{i2} - E_0^o(0) - E_0^o(t_f)$$

$$h^a = h_0^o + h_0^{i1} + h_0^{i2} - h_0^o(0) - h_0^o(t_f) \tag{47}$$

Results

The preceding algorithm was implemented into the NASA Ames Research Center code, ACSYNT. Minimum-fuel, -time, and direct operating cost cases were run for a modified Boeing[22] HSCT design. Additional information on the model can be found in Ref. 21. A range of 3000 n mile was chosen because it is approximately the distance from New York to London and this route is ideal for the HSCT. As will be made apparent later, this design could travel longer routes. Figure 1 illustrates the HSCT geometry and Table 1 lists some of its parameters.

Figure 2 shows altitude vs Mach number for the minimum-fuel case. The trajectory consists of three segments: ascent, cruise, and descent. The ascent contains two altitude jumps. The first occurs at Mach 1 and is due to the transonic D increase. This jump results in an altitude loss of about 10,000 ft. The second occurs at Mach 1.8 and is due to a temperature limit at the inlet of the engines. The remainder of the ascent trajectory follows the q boundary. The cruise lies on the maximum M boundary and is at maximum throttle. Thus, the two assumptions that were made in deriving the first-order weight/range dynamics are valid. During cruise, the vehicle gains about 10,000 ft of altitude. Finally, the descent is lofted, occurring high in the flight envelope and maximizing range. The flight envelope upper boundary is shown for comparison. It comprises stall and altitude limited sections. The upper boundary shifts as the vehicle decreases in weight. The vehicle weight at the end of the trajectory was used to calculate the upper boundary shown. Recall that the optimization function minimizes vD, which is similar to minimizing D because low v corresponds to low D (this only holds for regions of high M and h where the limiting constraint is loft ceiling, and, therefore, α must remain small). Furthermore, minimizing D at constant w is equivalent to maximizing L/D.

Calculation of idle is difficult due to its proximity to engine flame blow out. This causes the magnitude of T to be discontinuous at idle, and the guidance algorithm is sensitive to T. Thus, as seen in Fig. 2, there are small jumps in the descent trajectory.

Figure 3 displays altitude vs Mach number for the minimum-time case. Again, the trajectory consists of three segments. In this case, all of the segments lie on top of each other and follow the maximum q boundary of the flight envelope. This aspect appears because the minimum-time trajectory ascends and descends at maximum specific excess power, and maximum specific excess power is achieved in the flight envelope at the q boundary. Moreover, cruise lies at a single point on the M boundary. Cruise does not gain altitude because by gaining altitude the trajectory also gains energy, and gains in energy during cruise cause increases of flight time during descent. Finally, minimum-time ascent contains the same two altitude jumps

Table 1 HSCT parameters

Parameter	Value	Parameter	Value
Gross weight	759,300 lb	Wing planform area	5,500 ft^2
Fuel weight	416,685 lb	Wingspan	137.35 ft
Payload		Leading-edge sweep	48 deg
First-class passengers	30	Aspect ratio	3.43
Coach-class passengers	274	Body length	314 ft
Flight crew	2	Maximum M	2.4
Flight attendants	9	Maximum q	1,000 lb/ft^2

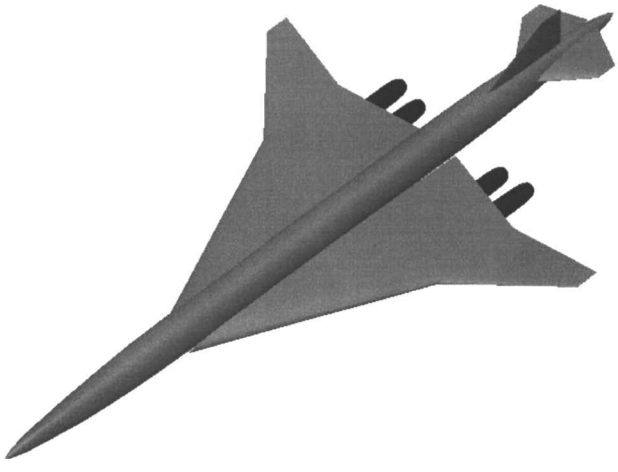

Fig. 1 HSCT geometry.

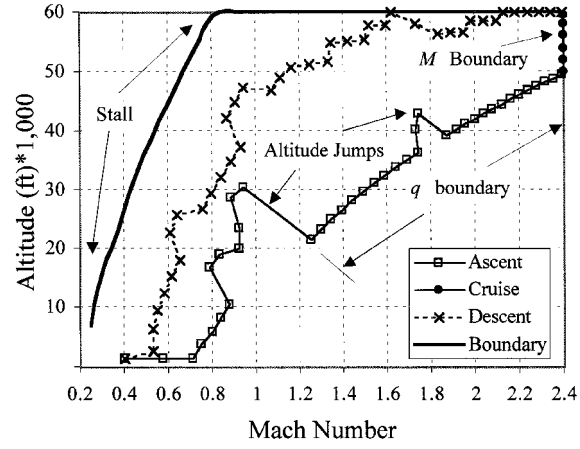

Fig. 2 Minimum-fuel trajectory.

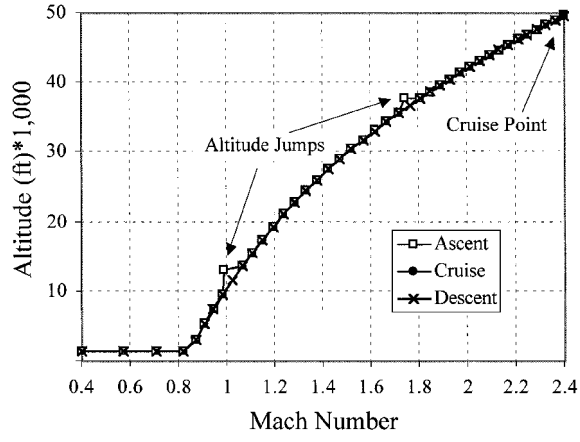

Fig. 3 Minimum-time trajectory.

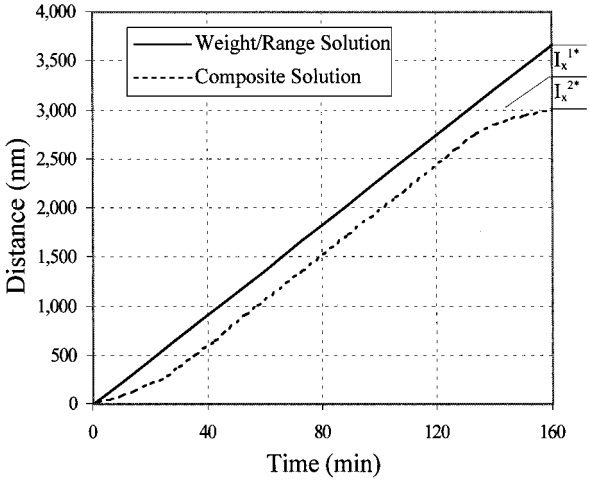

Fig. 4 Distance vs time.

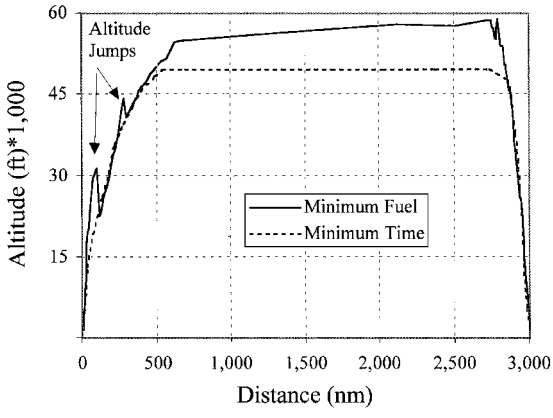

Fig. 5 Altitude vs distance.

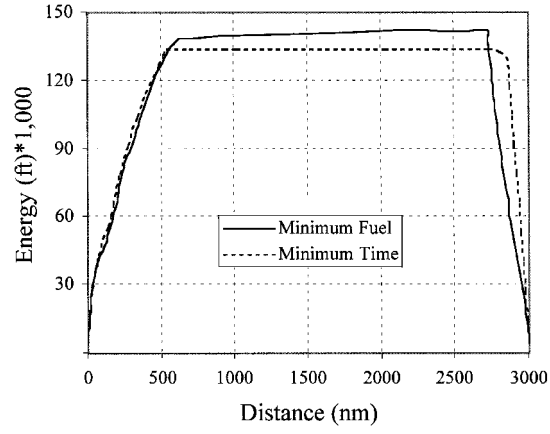

Fig. 6 Energy height vs distance.

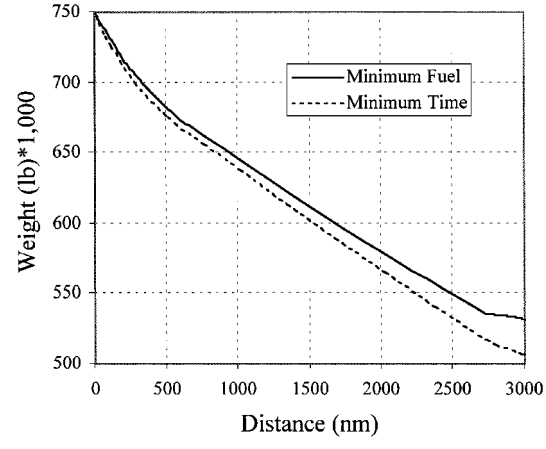

Fig. 7 Aircraft weight vs distance.

as minimum-fuel ascent. In this case, however, the jumps are very small.

Figure 4 shows distance vs time for the minimum-fuel case. Here, both the weight/range dynamics and composite solutions are plotted to illustrate the additive composition process. Recall that the weight/range dynamics solution ignores ascent and descent by beginning and ending at the optimal cruise altitude and energy. Therefore, it appears linear in Fig. 4. Conversely, the composite solution accounts for ascent and descent by the way it diverges from the weight/range dynamics solution at the beginning, follows it in the middle, and diverges from it again at the end. Furthermore, the flight time is the same for both solutions, indicating that the additive composition process does not modify the independent variable t. On the other hand, the dependent variable x is corrected for ascent and descent by the process. As illustrated, I_x^{1*} and I_x^{2*} [see Eqs. (44)] are magnitudes of the corrections. The other state and control dependent variables are also corrected similarly. The independence of t on the additive composite procedure suggests that x would be a good choice of independent variable for future analysis.

Figures 5 and 6 show altitude and energy height vs distance for both minimum time and minimum fuel. The timescale separation of h and E is illustrated by large changes in both variables occurring at the beginning and end of the trajectories, with periods of little change in the middle. Additionally, during cruise, minimum-fuel trajectories gain h and E, whereas minimum-time trajectories maintain constant h and E. Finally, note that altitude jumps are visible on the minimum-fuel ascent in Fig. 6.

Figures 7 and 8 illustrate weight and flight time vs distance for both cases. Again, timescale separation is shown. The solutions are linear in the middle, where they model the weight/range dynamics, and are smoothly curved at the ends, where they model energy dynamics. Moreover, the minimum-fuel case consumes less fuel, and the minimum-time case uses less flight time. The derivatives of the curves in Fig. 7 appear discontinuous at points toward their ends because that is where the vehicle transitioned from full throttle to idle to begin descent. Finally, Fig. 7 shows that the trajectories only consume approximately 225,000 lb of fuel. According to Table 1, this amount of fuel is only a fraction of the fuel available; thus, the vehicle could travel much farther if needed. Alternatively, the vehicle could take off with less fuel and could travel the same distance more fuel efficiently.

In addition, a minimum direct operating cost trajectory was generated. Values of K_1 and K_2 were computed to approximate actual costs to the airline. The values were found to be $K_1 = 0.94$ dollars/s and $K_2 = 0.105$ dollars/lb fuel. At these values, the minimum direct operating cost trajectory was found to be very similar to the minimum-fuel trajectory. This is because there is a larger relative cost savings obtained by the minimum-fuel trajectory than the relative cost savings obtained by the minimum-time trajectory. For example, relative cost savings for the trajectories can be estimated by taking fuel and time differences from Figs. 7 and 8 and multiplying them by their corresponding costs:

$$25{,}000 \text{ lb} \times 0.105 \text{ dollars/lb} = \$2625 \text{ (relative savings, minimum-fuel trajectory)}$$

$$15 \text{ min} \times 60 \text{ s/min} \times 0.94 \text{dollars/s} = \$846 \text{ (relative savings, minimum-time trajectory)}$$

For different aircraft and/or atmospheric models, the cost savings could be different, causing a different minimum-cost trajectory. Similarly, the vehicle flight constraints and range also affect the minimum-cost trajectory.

Although an exact optimal trajectory is not available for comparison with the two trajectories obtained here, there is reason to believe the trajectories are highly accurate. First, for high-performance aircraft, it was found in Refs. 11 and 13 that although the zero-order approximation gave very poor results, adding the first-order terms gave a performance estimate within 1% of the value determined

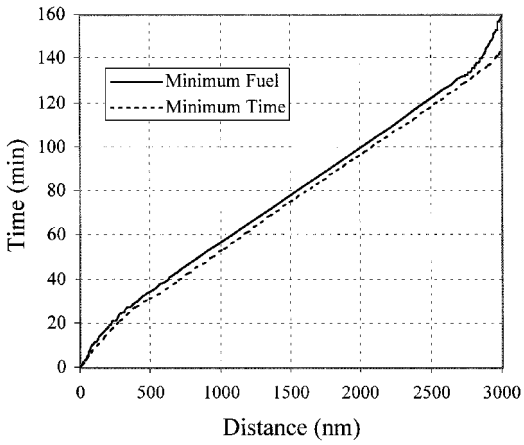

Fig. 8 Flight time vs distance.

by a steepest descent solution. Second, for low-performance subsonic transport aircraft, the zero-order algorithm of Refs. 17–19 was found to be sufficiently accurate for performance estimation and even onboard guidance. Indeed, the first-order corrections of the present paper are quite small, indicating a high degree of asymptotic approximation.

Concluding Remarks

A guidance algorithm for generating fixed-range near-optimal trajectories of HSCT has been developed. The optimal trajectories minimize flight time, fuel, or direct operating cost. The guidance algorithm calculates the controls in feedback form, that is, as a function of the current states. Its robustness and simplicity make it ideal for implementation into an aircraft design synthesis code such as ACSYNT.

The methodology is based on application of the maximum principle to a singularly perturbed dynamic model. The resulting 2PBVP is timescale separated into two systems of equations: the weight/range dynamics and the energy dynamics. The weight/range dynamics model the cruise segment of the trajectory, whereas the energy dynamics model the ascent and descent segments of the trajectory. Each system of equations is expanded and solved to first order. The solutions are then combined into a composite solution approximating the solution of the equations of motion.

Results show that minimum-fuel trajectories consist of minimum-fuel energy climbs, cruise climbs, and maximum L/D descents. Minimum-time trajectories consist of maximum specific excess power ascents and descents and constant altitude cruises. In our study, the minimum direct operating cost trajectory was nearly identical to the minimum-fuel trajectory.

Appendix A: Zero-Order Range Dynamics

The state equations are

$$\frac{\mathrm{d}w_0^o}{\mathrm{d}t} = -\beta_0^o, \qquad \frac{\mathrm{d}x_0^o}{\mathrm{d}t} = v_0^o, \qquad 0 = v_0^o F_0^o$$

$$0 = \gamma_0^o v_0^o, \qquad 0 = \frac{g}{v_0^o}\left(N_0^o - 1\right) \tag{A1}$$

and the adjoint equations are

$$\frac{\mathrm{d}\bar{\lambda}_0^o}{\mathrm{d}t} = -\lambda_{E0}^o v_0^o F_{w0}^o, \qquad \frac{\mathrm{d}\lambda_{x0}^o}{\mathrm{d}t} = 0$$

$$0 = \bar{\lambda}_0^o \beta_{E0}^o - \lambda_{x0}^o v_{E0}^o - \lambda_{E0}^o\left(v_{E0}^o F_0^o + v_0^o F_{E0}^o\right) - \lambda_{h0}^o \gamma_0^o v_{E0}^o + \lambda_{\gamma_0}^o \frac{g}{v_0^{o^2}}\left(N_0^o - 1\right) v_{E0}^o$$

$$0 = \bar{\lambda}_0^o \beta_{h0}^o - \lambda_{x0}^o v_{h0}^o - \lambda_{E0}^o\left(v_{h0}^o F_0^o + v_0^o F_{h0}^o\right) - \lambda_{h0}^o \gamma_0^o v_{h0}^o + \lambda_{\gamma_0}^o \frac{g}{v_0^{o^2}}\left(N_0^o - 1\right) v_{h0}^o$$

$$0 = -\lambda_{h0}^o v_0^o \tag{A2}$$

Appendix B: First-Order Range Dynamics

The state equations are

$$\frac{\mathrm{d}w_1^o}{\mathrm{d}t} = -\beta_1^o, \qquad \frac{\mathrm{d}x_1^o}{\mathrm{d}t} = v_1^o, \qquad \frac{\mathrm{d}E_0^o}{\mathrm{d}t} = v_1^o F_0^o + v_0^o F_1^o$$

$$0 = \gamma_1^o v_0^o + \gamma_0^o v_1^o, \qquad 0 = \frac{g}{v_0^o}\left(N_1^o - \frac{N_0^o - 1}{v_0^o} v_1^o\right) \tag{B1}$$

and the adjoint equations are

$$\frac{\mathrm{d}\bar{\lambda}_1^o}{\mathrm{d}t} = -\lambda_{E1}^o v_0^o F_{w0}^o - \lambda_{E0}^o\left(v_1^o F_{w0}^o + v_0^o F_{w1}^o\right), \qquad \frac{\mathrm{d}\lambda_{x1}^o}{\mathrm{d}t} = 0$$

$$\frac{\mathrm{d}\lambda_{E0}^o}{\mathrm{d}t} = \bar{\lambda}_1^o \beta_{E0}^o + \bar{\lambda}_0^o \beta_{E1}^o - \lambda_{x1}^o v_{E0}^o - \lambda_{x0}^o v_{E1}^o - \lambda_{E1}^o\left(v_{E0}^o F_0^o + v_0^o F_{E0}^o\right) - \lambda_{E0}^o\left(v_{E1}^o F_0^o + v_{E0}^o F_1^o + v_1^o F_{E0}^o + v_0^o F_{E1}^o\right) - \lambda_{h1}^o \gamma_0^o v_{E0}^o - \lambda_{h0}^o\left(\gamma_1^o v_{E0}^o + \gamma_0^o v_{E1}^o\right) + \lambda_{\gamma_1}^o \frac{g}{v_0^{o^2}}\left(N_0^o - 1\right) v_{E0}^o + \lambda_{\gamma_0}^o \frac{g}{v_0^{o^2}}\left[-2\frac{N_0^o - 1}{v_0^o} v_{E0}^o v_1^o + N_1^o v_{E0}^o + \left(N_0^o - 1\right) v_{E1}^o\right]$$

$$0 = \bar{\lambda}_1^o \beta_{h0}^o + \bar{\lambda}_0^o \beta_{h_1}^o - \lambda_{x1}^o v_{h0}^o - \lambda_{x0}^o v_{h1}^o - \lambda_{E1}^o\left(v_{h0}^o F_0^o + v_0^o F_{h0}^o\right) - \lambda_{E0}^o\left(v_{h1}^o F_0^o + v_{h0}^o F_1^o + v_1^o F_{h0}^o + v_0^o F_{h1}^o\right) - \lambda_{h1}^o \gamma_0^o v_{h0}^o - \lambda_{h0}^o\left(\gamma_1^o v_{h0}^o + \gamma_0^o v_{h1}^o\right) + \lambda_{\gamma_1}^o \frac{g}{v_0^{o^2}}\left(N_0^o - 1\right) v_{h0}^o + \lambda_{\gamma_0}^o \frac{g}{v_0^{o^2}}\left[-2\frac{N_0^o - 1}{v_0^o} v_{h0}^o v_1^0 + N_1^o v_{h0}^o + \left(N_0^o - 1\right) v_{h1}^o\right]$$

$$0 = -\lambda_{h1}^o v_0^o - \lambda_{h0}^o v_1^o \tag{B2}$$

Appendix C: Zero-Order Energy Dynamics

The state equations are

$$\frac{\mathrm{d}w_0^i}{\mathrm{d}\tau} = 0, \qquad \frac{\mathrm{d}x_0^i}{\mathrm{d}\tau} = 0, \qquad \frac{\mathrm{d}E_0^i}{\mathrm{d}\tau} = v_0^i F_0^i$$

$$0 = \gamma_0^i v_0^i, \qquad 0 = \frac{g}{v_0^i}\left(N_0^i - 1\right) \tag{C1}$$

and the adjoint equations are

$$\frac{\mathrm{d}\bar{\lambda}_0^i}{\mathrm{d}\tau} = 0, \qquad \frac{\mathrm{d}\lambda_{x0}^i}{\mathrm{d}\tau} = 0$$

$$\frac{\mathrm{d}\lambda_{E0}^i}{\mathrm{d}\tau} = \bar{\lambda}_0^i \beta_{E0}^i - \lambda_{x0}^i v_{E0}^i - \lambda_{E0}^i\left(v_{E0}^i F_0^i + v_0^i F_{E0}^i\right) - \lambda_{h0}^i \gamma_0^i v_{E0}^i + \lambda_{\gamma_0}^i \frac{g}{v_0^{i^2}}\left(N_0^i - 1\right) v_{E0}^i$$

$$0 = \bar{\lambda}_0^i \beta_{h0}^i - \lambda_{x0}^i v_{h0}^i - \lambda_{E0}^i\left(v_{h0}^i F_0^i + v_0^i F_{h0}^i\right) - \lambda_{h0}^i \gamma_0^i v_{h0}^i + \lambda_{\gamma_0}^i \frac{g}{v_0^{i^2}}\left(N_0^i - 1\right) v_{h0}^i$$

$$0 = -\lambda_{h0}^i v_0^i \tag{C2}$$

Appendix D: First-Order Energy Dynamics

The state equations are

$$\frac{\mathrm{d}w_1^i}{\mathrm{d}\tau} = -\beta_0^i, \qquad \frac{\mathrm{d}x_1^i}{\mathrm{d}\tau} = v_0^i, \qquad \frac{\mathrm{d}E_1^i}{\mathrm{d}\tau} = v_1^i F_0^i + v_0^i F_1^i$$

$$\frac{\mathrm{d}h_0^i}{\mathrm{d}\tau} = \gamma_1^i v_0^i + \gamma_0^i v_1^i, \qquad \frac{\mathrm{d}\gamma_0^i}{\mathrm{d}\tau} = \frac{g}{v_0^i}\left(N_1^i - \frac{N_0^i - 1}{v_0^i} v_1^i\right) \tag{D1}$$

and the adjoint equations are

$$\frac{d\bar{\lambda}_1^i}{d\tau} = -\lambda_{E0}^i v_0^i F_{w0}^i \qquad \frac{d\lambda_{x1}^i}{d\tau} = 0$$

$$\frac{d\lambda_{E1}^i}{d\tau} = \bar{\lambda}_1^i \beta_{E0}^i + \bar{\lambda}_0^i \beta_{E1}^i - \lambda_{x1}^i v_{E0}^i - \lambda_{x0}^i v_{E1}^i - \lambda_{E1}^i \left(v_{E0}^i F_0^i + v_0^i F_{E0}^i\right)$$
$$- \lambda_{E0}^i \left(v_{E1}^i F_0^i + v_{E0}^i F_1^i + v_1^i F_{E0}^i + v_0^i F_{E1}^i\right) - \lambda_{h1}^i \gamma_0^i v_{E0}^i$$
$$- \lambda_{h0}^i \left(\gamma_1^i v_{E0}^i + \gamma_0^i v_{E1}^i\right) + \lambda_{\gamma_1}^i \frac{g}{v_0^{i2}} \left(N_0^i - 1\right) v_{E0}^i$$
$$+ \lambda_{\gamma_0}^i \frac{g}{v_0^{i2}} \left[-2 \frac{N_0^i - 1}{v_0^i} v_{E0}^i v_1^i + N_1^i v_{E0}^i + \left(N_0^i - 1\right) v_{E1}^i\right]$$

$$\frac{d\lambda_{h0}^i}{d\tau} = \bar{\lambda}_1^i \beta_{h0}^i + \bar{\lambda}_0^i \beta_{h1}^i - \lambda_{x1}^i v_{h0}^i - \lambda_{x0}^i v_{h1}^i - \lambda_{E1}^i \left(v_{h0}^i F_0^i\right.$$
$$\left. + v_0^i F_{h0}^i\right) - \lambda_{E0}^i \left(v_{h1}^i F_0^i + v_{h0}^i F_1^i + v_1^i F_{h0}^i + v_0^i F_{h1}^i\right)$$
$$- \lambda_{h1}^i \gamma_0^i v_{h0}^i - \lambda_{h0}^i \left(\gamma_1^i v_{h0}^i + \gamma_0^i v_{h1}^i\right) + \lambda_{\gamma_1}^i \frac{g}{v_0^{i2}} \left(N_0^i - 1\right) v_{h0}^i$$
$$+ \lambda_{\gamma_0}^i \frac{g}{v_0^{i2}} \left[-2 \frac{N_0^i - 1}{v_0^i} v_{h0}^i v_1^i + N_1^i v_{h0}^i + \left(N_0^i - 1\right) v_{h1}^i\right]$$

$$\frac{d\lambda_{\gamma 0}^i}{d\tau} = -\lambda_{h1}^i v_0^i - \lambda_{h0}^i v_1^i \tag{D2}$$

Appendix E: Necessary Conditions

The zero-order equations are

$$K_1 + \bar{\lambda}_0 \beta_0 = \lambda_{x0} v_0 + \lambda_{E0} v_0 F_0 + \lambda_{h0} v_0 \gamma_0 + \lambda_{\gamma 0} (g/v_0)(N_0 - 1)$$
$$\lambda_{E0} v_0 F_{N0} = -\lambda_{\gamma 0} (g/v_0), \qquad \bar{\lambda}_0 \beta_{\pi 0} = \lambda_{E0} v_0 F_{\pi 0} \tag{E1}$$

and the first-order equations are

$$\bar{\lambda}_1 \beta_0 + \bar{\lambda}_0 \beta_1 = \lambda_{x1} v_0 + \lambda_{x0} v_1 + \lambda_{E1} v_0 F_0 + \lambda_{E0} (v_1 F_0 + v_0 F_1)$$
$$+ \lambda_{h1} v_0 \gamma_0 + \lambda_{h0} (v_1 \gamma_0 + v_0 \gamma_1) + \lambda_{\gamma_1} (g/v_0)(N_0 - 1)$$
$$+ \lambda_{\gamma 0} (g/v_0)\{N_1 - [(N_0 - 1)/v_0] v_1\}$$
$$\lambda_{E1} v_0 F_{N0} + \lambda_{E0} (v_1 F_{N0} + v_0 F_{N1}) = (g/v_0)[\lambda_{\gamma 0} (v_1/v_0) - \lambda_{\gamma_1}]$$
$$\bar{\lambda}_1 \beta_{\pi 0} + \bar{\lambda}_0 \beta_{\pi 1} = \lambda_{E1} v_0 F_{\pi 0} + \lambda_{E0} (v_1 F_{\pi 0} + v_0 F_{\pi 1}) \tag{E2}$$

Acknowledgment

This research was supported by the NASA Ames Research Center, Grant NCC2-5250.

References

[1] Scott, P., "Sonic Bust," *Scientific American*, Vol. 283, No. 3, 2000, p. 44.

[2] Wilhite, A., and Shaw, R., "HSCT Research Picks Up Speed," *Aerospace America*, Vol. 35, No. 8, 1997, pp. 24–29.

[3] Seebass, R., "History and Economics of, and Prospects for, Commercial Supersonic Transport," *Fluid Dynamics Research on Supersonic Aircraft*, Research and Technology Organization Paper RTO-EN-4 AC/323(AVT)TP/6, Nov. 1998, pp.1-1–1-6.

[4] Myklebust, A., and Gelhausen, P., "Putting the ACSYNT on Aircraft Design," *Aerospace America*, Vol. 32, No. 9, 1994, pp. 26–30.

[5] Ardema, M., Windhorst, R., and Phillips, J., "Optimization of Supersonic Transport Trajectories," NASA TM-112223, March 1998.

[6] Bryson, A., Jr., Desai, M., and Hoffman, W., "Energy-State Approximation in Performance Optimization of Supersonic Aircraft," *Journal of Aircraft*, Vol. 6, No. 6, 1969, pp. 481–487.

[7] Kelly, H., and Edelbaum, T., "Energy Climbs, Energy Turns, and Asymptotic Expansions," *Journal of Aircraft*, Vol. 7, No. 1, 1970, pp. 93–95.

[8] Kelly, H., "Aircraft Maneuver Optimization by Reduced-Order Approximation," *Control and Dynamic Systems*, Vol. 10, edited by C. T. Leondes, Academic, New York, 1973, pp. 131–178.

[9] Kelly, H., Cliff, E., and Weston, A., "Energy State Revisited," *Optimal Control Applications and Methods*, Vol. 7, No. 2, 1986, pp. 195–200.

[10] Ardema, M., and Rajan, N., "Slow and Fast State Variables in Three-Dimensional Flight Dynamics," *Journal of Guidance, Control, and Dynamics*, Vol. 8, No. 4, 1985, pp. 532–535.

[11] Ardema, M., "Singular Perturbations in Flight Mechanics," NASA TM X-62,380, July 1977.

[12] Ardema, M., "An Introduction to Singular Perturbations in Nonlinear Optimal Control," *Singular Perturbations in Systems and Control*, International Center for Mechanical Sciences Courses and Lectures, Vol. 280, Springer-Verlag, New York, 1983, pp. 1–92.

[13] Ardema, M., "Solution of the Minimum-Time-to-Climb Problem by Matched Asymptotic Expansions," *AIAA Journal*, Vol. 14, No. 7, 1976, pp. 843–850.

[14] Calise, A., "Singular Perturbation Methods for Variational Problems in Aircraft Flight," *IEEE Transactions on Automatic Control*, Vol. AC-21, No. 3, 1976, pp. 345–353.

[15] Calise, A., "Extended Energy Management Methods for Flight Performance Optimization," *AIAA Journal*, Vol. 15, No. 3, 1977, pp. 314–321.

[16] Calise, A., "A New Boundary Layer Matching Procedure for Singularly Perturbed Systems," *IEEE Transactions on Automatic Control*, Vol. AC-23, No. 3, 1978, pp. 434–438.

[17] Erzberger, H., and Lee, H., "Algorithm for Fixed-Range Optimal Trajectories," NASA TP-1565, July 1980.

[18] Erzberger, H., "Automation of On-Board Flight Path Management," NASA TM-84212, Dec. 1981.

[19] Erzberger, H., "Optimum Climb and Descent Trajectories for Airline Missions," *Theory and Applications of Optimal Control in Aerospace Systems*, AGARD, AGARDograph 251, July 1981, pp. 9-1–9-15.

[20] Aggarwal, R., Calise, A., and Goldstein, F., "Singular Perturbation Analysis of Optimal Flight Profiles for Transport Aircraft," Joint Automatic Control Conf., Dynamics Research Corp., Paper TP26–4:50, Wilmington, MA, June 1977.

[21] Windhorst, R., and Ardema, M., "Optimization of Fixed-Range Trajectories for Supersonic Transport Aircraft," Ph.D. Dissertation, Mechanical Engineering Dept., Santa Clara Univ., Santa Clara, CA, March 1999.

[22] Boeing Commercial Airplanes, "High-Speed Civil Transport Study," NASA CR-4233, Sept. 1989.